optica

Noise-mediated Casimir-like pulse interaction mechanism in lasers

Rafi Weill,[1] Alexander Bekker,[1] Vladimir Smulakovsky,[1] Baruch Fischer,[1,3] and Omri Gat[2,*]

[1]Department of Electrical Engineering, Technion, Haifa 32000, Israel
[2]Racah Institute of Physics, Hebrew University, Jerusalem 91904, Israel
[3]e-mail: fischer@ee.technion.ac.il
*Corresponding author: omrigat@mail.huji.ac.il

Received 11 November 2015; revised 22 December 2015; accepted 22 December 2015 (Doc. ID 249807); published 16 February 2016

Strongly pumped mode-locked lasers often form pulse bunches. Although several mechanisms of pulse interaction are known, none yields the experimentally observed long-range attraction. Here we demonstrate theoretically and experimentally a new pulse interaction mechanism mediated by the continuum noise floor that is a universal feature in multipulse passively mode-locked lasers. Long-range attraction is facilitated by the depletion of the gain by the pulses, leading to an inhomogeneous noise floor that biases the timing jitter of the pulses and produces an effective interpulse potential with stable pulse bunch configurations. The pulses attract by suppressing electromagnetic fluctuations, as do conductors in the Casimir effect of quantum electrodynamics. This enables manipulation and design of multipulse waveforms to ultimately make them useful for application of mode-locked lasers.

OCIS codes: (140.4050) Mode-locked lasers; (140.7090) Ultrafast lasers; (140.3538) Lasers, pulsed.

http://dx.doi.org/10.1364/OPTICA.3.000189

Passively mode-locked lasers (PMLs), pumped by sufficient power and operating with anomalous dispersion, usually demonstrate multipulse operation, in which there are several pulses propagating in the cavity at the same time. Once formed, these pulses exhibit very rich dynamics, including random motion [1], formation of equally spaced configurations (harmonic PML) [2,3], and the formation of ordered pulse bunches [4–9], with spacing ranging from picoseconds to nanoseconds.

Despite intense research effort, the laws governing pulse interactions in PML are only partially known. Interaction mechanisms identified so far belong to four classes. The first is coherent overlap, which locks both the relative timing and phase of neighboring pulses [5,7,10]. Second is the deceleration of trailing pulses caused by gain depletion of the leading pulses that produces long-range repulsive interactions, which drive the pulses to an evenly spaced configuration, commonly observed in semiconductor lasers [3]. The third are interactions in fiber lasers mediated by acoustic waves generated by electrostriction [11,12], which can be both attractive and repulsive at long range. The fourth mechanism is the medium-range interaction mediated by dispersive waves [1,2,4] that accumulate at resonant sideband frequencies by cw radiation emitted from pulses and lead to the formation of low-intensity pulse pedestals [13–15].

The main deficiency of existing theories of pulse interactions in laser cavities is that none implies the universal long-range attraction necessary to generate pulse bunches from an initial random pulse configuration. In this Letter, we resolve this issue by putting forward a universal pulse attraction mechanism induced by the interaction of the pulses with the *continuum noise floor*, combined with the saturation of the gain by the pulses. Moreover, the interaction becomes *repulsive* when the separation between pulses in the bunch decreases until it is comparable to the width of the aforementioned dispersive-wave pedestals, implying equilibrium pulse separation of tens to hundreds of picoseconds, depending on the pedestal width, in excellent agreement with experimental observation in fiber PMLs.

The pulse interaction derived here is a result of the timing jitter. When noise is homogeneous, the jitter is unbiased. However, depletion of the gain medium weakens the noise in the wake of an ultrashort pulse, *biasing* the jitter and giving rise to pulse drift, which is universally attractive at large separations.

This noise-mediated pulse interaction is reminiscent of the Casimir effect in quantum electrodynamics [16], in that both interactions arise from the suppression of fluctuations of the electromagnetic field, although the details are different.

Our analysis is based on the many-body theory of passive mode locking, in which the steady state of the laser subject to noise is studied as a statistical mechanics system of interacting modes [17–23]. It shows, in particular, that the onset of mode locking is a thermodynamic phase transition, and that when the cavity power is increased beyond the absorber saturation point, additional pulses form in a cascade of transitions between thermodynamic phases labeled by the number of pulses [8,9].

Here we augment the theory by accounting for gain saturation, which produces the noise floor inhomogoneity essential for noise-mediated interactions. The pulse timing fluctuation statistics are derived from their overlap interaction with the noise floor [24]. The resulting effective interpulse potential implies bunching with pulse separations close to the pedestal width. The theoretical

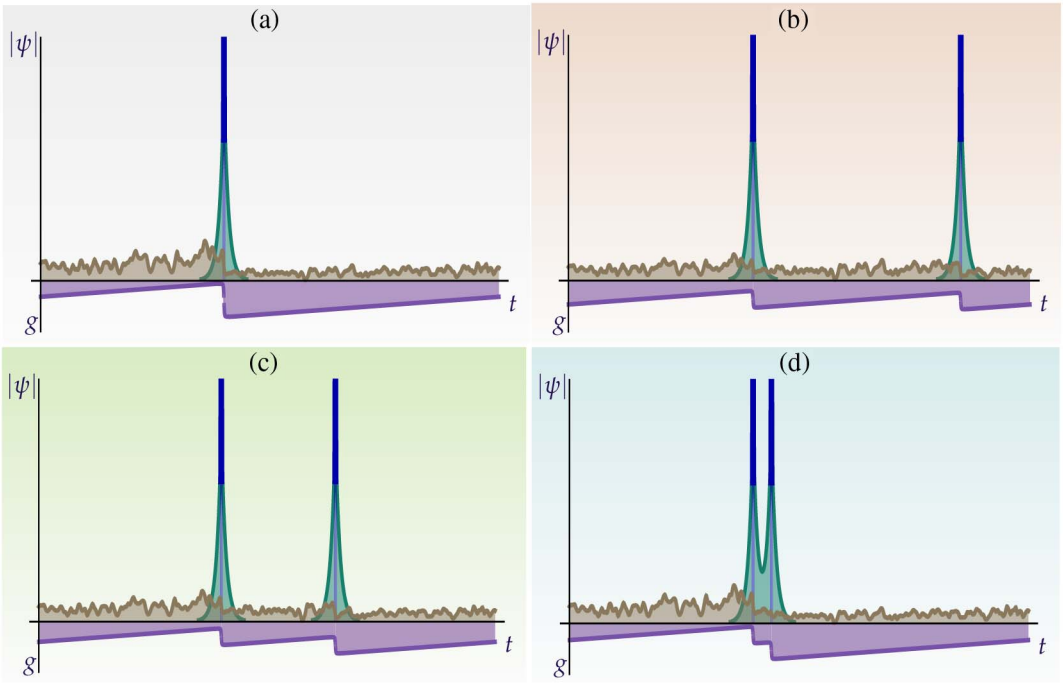

Fig. 1. Schematic of the pulse bunching process. (a) A single pulse configuration (b) becomes unstable to the formation of a second pulse at a random cavity position, (c) which is then attracted to the second pulse by noise interaction (d) until it reaches a steady state determined by pedestal overlap. The pulse, pedestal, and continuum waveforms are shown in blue, green, and brown, respectively. The (negative) net gain profile for the given separations is shown in violet. The pulse and pedestal widths are 0.001 and 0.01 round-trip time, respectively, and they saturate 70% and 20%, respectively, of the maximum gain. The pulse waveform is clipped at high powers for visibility.

analysis is supported by experiments in fiber PMLs, demonstrating the noise floor inhomogeneity and its response to pulse motion.

Optical pulses interact not only in lasers, and recent work has demonstrated interactions in pumped nonlinear resonators. Reference [25] studied acoustic-mediated interactions in fiber resonators, identifying intervals of attraction and repulsion, and [26,27] studied overlap interactions. The latter mechanism in resonators is different from laser interactions because, unlike mode-locked lasers, the waveform of nonlinear resonators contains a strong cw component, which can mediate long-range interaction.

We model the dynamics of the laser waveform $\psi(t,z)$ by the Haus master equation:

$$\partial_z\psi = i(\partial_t^2\psi + 2|\psi|^2\psi) + G[\psi] - L[\psi] + \Gamma(z,t), \qquad \textbf{(1)}$$

where the first two terms on the right model the chromatic dispersion and Kerr nonlinearity, $\Gamma(t,z)$ is a white-noise process modeling spontaneous emission and other noise sources, and G and L are the gain and loss operators, respectively, that take into account the depletion and slow recovery of the gain and the spatial the distribution of gain and loss in the cavity, in addition to the standard saturable absorption and gain spectral response terms [28,29]; see Supplement 1 for details.

The model includes the terms necessary for the full description of the laser waveform, which consists of pulses, dispersive wave pedestals generated from pulse scattering on discrete cavity elements [13,14], and the random quasi-cw floor generated by the noise. Although the laser equation [Eq. (1)] is nonlinear, these three components of the waveform combine approximately linearly, since they are characterized by different time scales. The pulse waveform ψ_a is a sum of N soliton-like pulses centered at times t_n with widths $t_a^{(n)} < 1$ ps; the pedestal waveform ψ_b is a sum of low-amplitude waves with frequencies near ω_n, $n = 1, \ldots, N$ determined by the Kelly–Gordon resonance condition [13,14], with envelopes centered at the pulses that decay exponentially on scales $t_b^{(n)} \sim 10$–1000 ps; and the continuum waveform ψ_c extends over the entire cavity with round-trip time $t_R > 10$ ns.

Unlike the pulse and pedestal that are weakly perturbed by the noise, the continuum waveform is noise generated. It must therefore be characterized by the continuum intensity $I_c = \langle|\psi_c|^2\rangle$, where $\langle\cdot\rangle$ signifies the noise-averaged expectation value. I_c is determined by the linear terms in Eq. (1), so that it inherits the time dependence of the gain $g(t)$, which is depleted by the pulses and pedestals and recovers in the interpulse periods.

Since the gain dynamics is typically very slow, $g(t)$ is approximately linear far from the pulses. As shown in Supplement 1, far from the pulses the continuum intensity I_c is proportional to $1/\sqrt{l - g(t)}$, where l is the linear loss. In contrast, near the pulses, gain depletion leads to a sharp decrease in the gain, so that $g(t_n^+) < g(t_n^-)$, where $g(t_n^\pm)$ stand for the gain just after and just before the nth pulse, respectively. Near the pulses, the continuum intensity changes more slowly than the gain, and its value at the center of the pulses, which determines the timing fluctuations, is proportional to $\frac{1}{2}(1/\sqrt{l - g(t_n^-)} + 1/\sqrt{l - g(t_n^+)})$. Figure 1 shows schematics of the pulse, pedestal, and continuum waveforms with the gain profile for single- and two-pulse states.

The profile of the continuum resulting from our theory has been verified by experiments in a fiber PML system (see Supplement 1 for details of the laser). Figure 2 shows oscillograms of the laser output signal of two consecutive round trips for several

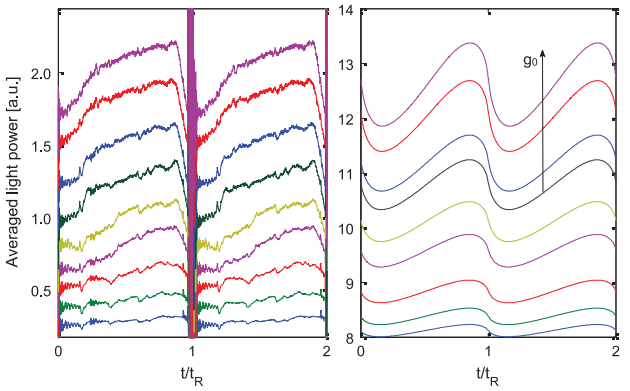

Fig. 2. Inhomogeneous continuum and its dependence on pumping. Experimental measurement (left) and theoretical calculation (right) of the continuum power in a multipulse PML for several pumping levels. The laser was injected with ∼0.6 mW of amplified spontaneous emission. The continuum power was measured by averaging output power over several hundred round trips; since the continuum is the only nonnegligible component of the waveform in more than 99% of the cavity, one can identify the output waveform with the continuum waveform, except near the sharp peak in the middle. Experimental graphs are ordered by increasing pumping from ∼12 to ∼45 mW and theoretical graphs by increasing mean gain g_0 from bottom to top, showing the increase of continuum power and its variation with increased pumping.

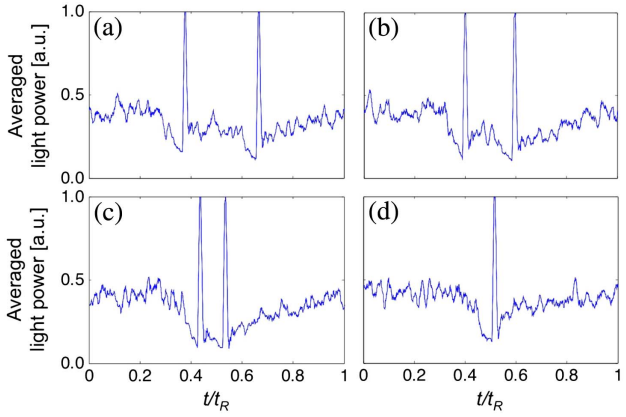

Fig. 3. Pulse motion and evolution of the continuum. A similar measurement to the one shown in Fig. 2 with a single pumping value, showing (a)–(c) three consecutive transient states and (d) the steady state. The experiment shows how the continuum power profile changes as the pulses approach each other to form the bunch, seen as a single peak in panel (d) due to the limited resolution of the oscilloscope.

pumping levels. The pulses and pedestals are localized near the center of the time axis and are not resolved temporally. Most of the pulse waveform is clipped to focus on the weaker continuum waveform. The measurements are compared to numerical calculations of the mean continuum power for several net gain values, exhibiting the variation of the continuum power caused by pulse-induced gain depletion. Chromatic dispersion makes the suppression of fluctuations extend before and after the pulses. The good agreement between experiment and theory shows that the continuum inhomogeneity is indeed a consequence of the gain dynamics.

The overlap interaction of each pulse with the local continuum waveform is a source of random timing jitter in the pulse timings t_n. The timing diffusion coefficient D_n is therefore proportional to the local continuum intensity $I_c(t_n)$ [24]. However, the inhomogeneity of the continuum *biases* the diffusion. To understand the effective drift arising from this bias, we note that the continuum dynamical time scale, of the order of a nanosecond, is much shorter than the millisecond time scale of relative pulse motion, so that the continuum intensity profile adjusts itself to the instantaneous pulse configuration.

This argument is supported by the experimental measurements of the *transient* evolution of the continuum waveform shown in Fig. 3. The measurements are obtained as those in Fig. 2, but are taken just after the seeding of a new pulse, probing *transient* approach to steady state. The graphs show that each pulse creates a gain shadow, and that the continuum intensity responds to the instantaneous gain profile (note that because of clipping and limited oscilloscope resolution, the two pulses appear as one peak in the steady state shown in the last panel).

In effect, therefore, the pulses in multipulse waveforms perform Brownian motion with timing-dependent diffusion coefficients $D_n(t_1, \ldots, t_N)$. It follows from standard theory of biased Brownian motion [30] that the drift velocity of the nth pulse is

$$\frac{\partial\langle t_n\rangle}{\partial z} = \frac{1}{2}\frac{\partial D_n}{\partial t_n}. \tag{2}$$

For concrete calculations, we study the simplest case of a two-pulse waveform with identical pulse powers and pedestals. Global time translation invariance implies that D_1 and D_2 depend only on the separation time $t_s = t_2 - t_1$, and, therefore,

$$\frac{\partial\langle t_s\rangle}{\partial z} = \frac{1}{2}\frac{\partial D_s}{\partial t_s}, \qquad \text{with } D_s = D_1 + D_2. \tag{3}$$

The explicit form of D_s follows in a straightforward manner from the considerations and results presented above, as detailed in Supplement 1. Since D_s contains contributions from the two pulses, and the continuum intensity at each pulse is the average of two terms, D_s is a sum of four terms:

$$D_s(t_s) = \frac{1}{2}D_0(\kappa(\Delta_p, \Delta_b, \Delta_b) + \kappa(1 - \Delta_p, -\Delta_b, \Delta_b) + \kappa(\Delta_p - 1, \Delta_b, -\Delta_b) + \kappa(-\Delta_p, -\Delta_b, -\Delta_b)), \tag{4}$$

where Δ_p, Δ_b are the depletion of the gain by the pulse and pedestal, and by the pedestal only, respectively, divided by the mean gain, and

$$\kappa(\Delta_1, \Delta_2, \Delta_3) = (1 - \Delta_1\frac{t_s}{t_R} + \Delta_2 - \Delta_3(e^{-t_s/t_b} + e^{(t_s - t_R)/t_b}))^{-1/2}. \tag{5}$$

Here, t_R is again the laser round-trip time, and D_0 is the diffusion constant of a single pulse with the same mean gain.

Equation (4) obeys the obvious symmetries $D_s(t_s) = D_s(t_s + t_R) = D_s(-t_s)$, so we need to study it only in the interval $0 \le t_s \le t_R/2$, shown in Fig. 4. When pedestals are absent, corresponding to $\Delta_b = 0$ in Eq. (4), the effective potential $-\frac{1}{2}D_s$ is universally attractive, and the only minimum is at zero separation. However, gain depletion by the pedestals is a source of repulsion for pulse separations comparable to or smaller than the pedestal width, which together with the long-range attraction can form a stable equilibrium point in the interpulse potential. In the typical situation, where the pedestal width is much smaller than the round-trip time, the effective potential has a unique minimum at

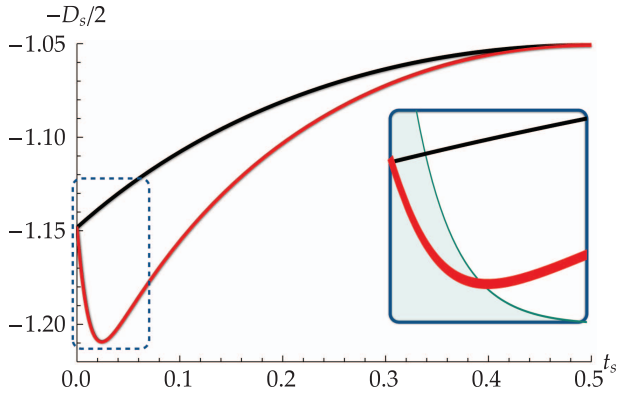

Fig. 4. Two-pulse noise-mediated interaction effective potential. The timing separation diffusion coefficient D_s times $-\frac{1}{2}$ (normalized by the single pulse diffusion coefficient D_0) as a function of the separation t_s (normalized by the cavity round-trip time t_R). The black (red) curve shows the interaction potential for pulses that deplete 70% of the net gain without (with) pedestals, whose width is 0.01 of the round-trip time, that deplete an additional 20% of the net gain. The latter displays a stable fixed point near $t_s = 0.024 t_R$. Inset: zoom on the small separation region that includes the minimum induced by the pedestal, overlaid with the pedestal waveform (green).

$$t_s^{(\mathrm{eq})} = t_b \log\left(\frac{\Delta_b}{\Delta_p}\frac{t_R}{t_b}\right) \tag{6}$$

if the value of the logarithm is positive. This result completes our demonstration that the noise-mediated interaction gives rise to pulse bunching of two-pulse waveforms, and that the steady-state separation is determined by the pedestal properties.

The key ingredients in the noise-mediated interaction mechanism are present in every PML system. Since it acts in conjunction with several other interactions, mentioned briefly above, the bunching is not always observed, and its properties are system dependent. Combining, if necessary, with the previously known interactions, the theory presented here enables the quantitative modeling of multipulse waveforms. Pulse shaping and control is an important field in ultrashort photonics and its applications [31]. Identification and control of the interaction mechanism can now lead to waveform shaping on the *bunch* level. opening exciting possibilities for applications of multipulse waveforms.

Funding. United States–Israel Binational Science Foundation (2010442); Israel Science Foundation (ISF).

See Supplement 1 for supporting content.

REFERENCES

1. D. Tang, B. Zhao, L. Zhao, and H. Tam, Phys. Rev. E **72**, 016616 (2005).
2. A. B. Grudinin and S. Gray, J. Opt. Soc. Am. B **14**, 144 (1997).
3. J. N. Kutz, B. C. Collings, K. Bergman, and W. H. Knox, IEEE J. Quantum Electron. **34**, 1749 (1998).
4. J. M. Soto-Crespo, N. Akhmediev, P. Grelu, and F. Belhache, Opt. Lett. **28**, 1757 (2003).
5. M. J. Lederer, B. Luther-Davies, H. H. Tan, C. Jagadish, N. N. Akhmediev, and J. M. Soto-Crespo, J. Opt. Soc. Am. B **16**, 895 (1999).
6. D. Tang, B. Zhao, D. Shen, C. Lu, W. Man, and H. Tam, Phys. Rev. A **66**, 033806 (2002).
7. P. Grelu, F. Belhache, F. Gutty, and J. M. Soto-Crespo, Opt. Lett. **27**, 966 (2002).
8. B. Vodonos, R. Weill, A. Gordon, A. Bekker, V. Smulakovsky, O. Gat, and B. Fischer, Phys. Rev. Lett. **93**, 153901 (2004).
9. R. Weill, B. Vodonos, A. Gordon, O. Gat, and B. Fischer, Phys. Rev. E **76**, 031112 (2007).
10. N. N. Akhmediev, A. Ankiewicz, and J. M. Soto-Crespo, J. Opt. Soc. Am. B **15**, 515 (1998).
11. E. M. Dianov, A. V. Luchnikov, A. N. Pilipetskii, and A. N. Starodumov, Opt. Lett. **15**, 314 (1990).
12. A. N. Pilipetskii, E. A. Golovchenko, and C. R. Menyuk, Opt. Lett. **20**, 907 (1995).
13. J. P. Gordon, J. Opt. Soc. Am. B **9**, 91 (1992).
14. S. Kelly, Electron. Lett. **28**, 806 (1992).
15. R. Weill, A. Bekker, V. Smulakovsky, B. Fischer, and O. Gat, Phys. Rev. A **83**, 043831 (2011).
16. H. Casimir, *Proceedings of the Koninklijke Nederlandse Akademie Van Wetenschappen* (1997), Vol. **100**, pp. 61–63 [Reprinted from Proceedings of the Koninklijke Nederlandse Akademie van Wetenschappen (1948), Vol 51, pp. 793-795].
17. A. Gordon and B. Fischer, Phys. Rev. Lett. **89**, 103901 (2002).
18. O. Gat, A. Gordon, and B. Fischer, Phys. Rev. E **70**, 046108 (2004).
19. A. Picozzi and M. Haelterman, Phys. Rev. Lett. **92**, 103901 (2004).
20. O. Gat, A. Gordon, and B. Fischer, New J. Phys. **7**, 151 (2005).
21. M. Katz, A. Gordon, O. Gat, and B. Fischer, Phys. Rev. Lett. **97**, 113902 (2006).
22. L. Angelani, C. Conti, G. Ruocco, and F. Zamponi, Phys. Rev. B **74**, 104207 (2006).
23. L. Leuzzi, C. Conti, V. Folli, L. Angelani, and G. Ruocco, Phys. Rev. Lett. **102**, 083901 (2009).
24. M. Katz, O. Gat, and B. Fischer, Opt. Lett. **35**, 297 (2010).
25. J. K. Jang, M. Erkintalo, S. G. Murdoch, and S. Coen, Nat. Photonics **7**, 657 (2013).
26. T. Herr, V. Brasch, J. D. Jost, C. Y. Wang, N. M. Kondratiev, M. L. Gorodetsky, and T. J. Kippenberg, Nat. Photonics **8**, 145 (2013).
27. C. Godey, I. V. Balakireva, A. Coillet, and Y. K. Chembo, Phys. Rev. A **89**, 063814 (2014).
28. H. A. Haus, IEEE J. Select. Top. Quantum Electron. **6**, 1173 (2000).
29. J. N. Kutz, SIAM Rev. **48**, 629 (2006).
30. H. Risken, *The Fokker-Planck Equation* (Springer, 1989).
31. A. M. Weiner, Opt. Commun. **284**, 3669 (2011).